Chemistry–A European Journal
Research Article
doi.org/10.1002/chem.202401545
Chemistry Europe
European Chemical Societies Publishing
www.chemeurj.org

THz-EPR-based Magneto-Structural Correlations for Cobalt(II) Single-Ion Magnets With Bis-Chelate Coordination

Maximilian H. Pohle,[a] Thomas Lohmiller,[b] Michael Böhme,[a] Michał Rams,[c] Sven Ziegenbalg,[a] Helmar Görls,[a] Alexander Schnegg,[d] and Winfried Plass*[a]

New cobalt(II)-based complexes with $[N_2O_2]$ coordination formed by two bis-chelate ligands were synthesized and characterized by a multi-technique approach. The complexes possess an easy-axis anisotropy ($D<0$) and magnetic measurements show a field-induced slow relaxation of magnetization. The spin-reversal barriers, i.e., the splitting of the two lowest Kramers doublets (U_{ZFS}), have been measured by THz-EPR spectroscopy, which allows to distinguish the two crystallographically independent species present in one of the complexes. Based on these experimental U_{ZFS} energies together with those for related complexes reported in literature, it was possible to establish magneto-structural correlations. U_{ZFS} linearly depends on the elongation parameter ε_T of the (pseudo-)tetrahedral coordination, which is given by the ratio between the average obtuse and acute angles at the cobalt(II) ion, while U_{ZFS} was found to be virtually independent of the twist angle of the chelate planes. With increasing deviation from the orthogonality of the latter, the rhombicity ($|E/D|$) increases.

Introduction

The observation of slow relaxation of magnetization in molecular systems, with the Mn_{12} cluster as the first reported example,[1] has sparked the development of an outstanding number of compounds with promising potential in the fields of quantum computing,[2–4] spintronics,[5–7] and most notable data storage.[8] As a general goal, research initially focused on multinuclear systems such as metal cluster compounds with the aim of achieving a high total spin S.[9–13] Over the past decade, however, the focus has shifted to mononuclear systems, so-called single-ion magnets (SIMs),[14–18] which enable a much larger magnetic anisotropy than comparable higher-nuclear compounds.[19,20]

Among the 3d transition metal ions, high-spin cobalt(II) is particularly suitable for the generation of SIM candidates, as it combines an inherently large spin–orbit coupling with a reasonably large number of unpaired electrons ($S=3/2$).[21] The resulting magnetic anisotropy of such a cobalt(II) system is given by the splitting of the ground state multiplet into two Kramers doublets separated by the associated spin-reversal barrier ($U_{ZFS}=2\sqrt{D^2+3E^2}$), which can be parameterized by an axial (D) and a rhombic (E) zero-field splitting (ZFS) parameter. In addition, it is advantageous for cobalt(II)-based compounds that a high degree of flexibility can be observed with regard to the coordination environment, i.e., the number, charge and type of donor atoms, as well as the resulting coordination geometries.[22] In order to manipulate or even tune the magnetic behavior of SIMs, it is crucial to understand the factors that can potentially influence the magnetic anisotropy. To achieve this, a sufficiently large set of reliable data is required that provides structural variations within a limited range of parameters, in particular the coordination number at the cobalt(II) ion. Among the largest groups of cobalt(II)-based SIMs reported in the literature are four-coordinated high-spin complexes with a non-planar geometry, for which a wide variety of coordination environments with homoatomic ($[N_4]$,[23–32] $[O_4]$,[33] $[S_4]$,[33–36] $[Se_4]$,[33,35,37] $[Te_4]$[37]) and heteroatomic donor sets ($[N_2O_2]$,[38–49] $[N_2X_2]$,[50–53] $[P_2X_2]$,[54–56] $[S_2X_2]$,[57] $[(O/S)NX_2]$[58] with X = Cl, Br, I) are known (Scheme 1).

Since the first reports, several magneto-structural correlations for specific examples of the latter group of tetracoordinate cobalt(II)-based complexes have been described in the literature, which are related to chemical or geometrical parameters

[a] M. H. Pohle, Dr. M. Böhme, Dr. S. Ziegenbalg, Dr. H. Görls, Prof. Dr. W. Plass
Institut für Anorganische und Analytische Chemie, Friedrich-Schiller-Universität Jena, Humboldtstraße 8, 07743 Jena (Germany)
E-mail: sekr.plass@uni-jena.de
[b] Dr. T. Lohmiller
EPR4 Energy Joint Lab, Department Spins in Energy Conversion and Quantum Information Science, Helmholtz Zentrum Berlin für Materialien und Energie GmbH, Albert-Einstein-Straße 16, 12489 Berlin (Germany)
and
Current address: Humboldt-Universität zu Berlin, Institut für Chemie, Brook-Taylor-Str. 2, 12489 Berlin (Germany)
[c] Dr. M. Rams
Institute of Physics, Jagiellonian University, 30-348 Kraków (Poland)
[d] Dr. A. Schnegg
EPR Research Group, Max Planck Institute for Chemical Energy Conversion, Stiftstraße 34–36, 45470 Mülheim an der Ruhr (Germany)

Supporting information for this article is available on the WWW under https://doi.org/10.1002/chem.202401545

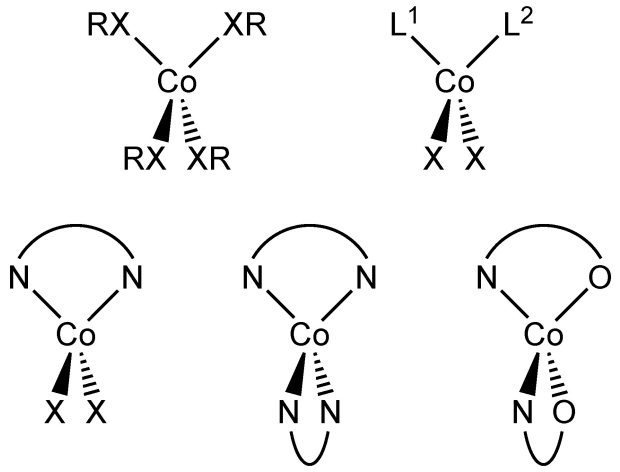

Scheme 1. Representation of the coordination environments of four-coordinate high-spin cobalt(II) complexes exhibiting SIM behavior.

and based either on the comparison of theoretical or experimental data:

(i) A clear correlation of the axial ZFS parameter *D* with the nature of the donor atoms, i.e., their softness, was found for three different types of donor environments, namely $[Co(Pn)_2X_2]$ (*Pn* = N, P, and As),[56] $[Co(Ch)(MeCN)X_2]$ (*Ch* = O and S),[58] and $[Co(ChR)_4]^{2-}$ (*Ch* = O, S, Se, and Te),[59] the latter based on *ab initio* calculations. In fact, it is found that heavier donor atoms lead to larger negative *D* values.

(ii) For the latter examples with $[S_4]$ donor environment, structural parameters affecting the ZFS were also identified by theoretical considerations and, in particular, it was found that elongation of the tetrahedral coordination along an S_4 axis leads to a larger negative axial ZFS parameter *D*.[36,60]

(iii) For complexes with $[N_2Cl_2]$ donor set, the distortion of the pseudotetrahedral coordination has been proposed to be described by the pair of N–Co–N and Cl–Co–Cl angles, leading to the theoretical prediction that angles smaller than the tetrahedral angle ($\angle T_d = 109.47^\circ$) lead to negative *D* values.[61] However, the authors stated that the experimental data shows a clear discrepancy with the theoretical model.

(iv) The previous correlation was later also adopted for complexes with $[S_2X_2]$ donor set (X=Cl, Br, and I) to describe their elongation along the corresponding pseudo-C_2 axis by a parameter given as $[2\times\angle T_d - (\angle S\text{–}Co\text{–}S + \angle X\text{–}Co\text{–}X)]$. Theoretical studies showed that a larger negative *D* value is expected when this parameter is increased.[62,63] This again indicates that an increased elongation of the tetrahedral coordination results in larger negative *D* values.

(v) A more general approach has been reported for complexes with an $[N_4]$ donor set at the cobalt(II) ion with two asymmetric bidentate chelate ligands following the concept of continuous symmetry measures (CSM).[28] For the then known complexes with $[N_4]$ coordination environment, this leads to a V-shaped correlation, which suggests the existence of an optimal symmetry requirement for structures with large negative *D* values with a narrow interval of CSM values.

(vi) In 2021, two reports on new complexes with $[N_4]$ coordination at the cobalt(II) ion using symmetric bidentate chelating ligands have appeared, which also emphasize the need for an optimal structure to generate a large negative *D* value.[29,30] In these cases, the bite angle of the chelate ligands was employed as structural parameter for the correlation, however, leading to different ideal values for the N–Co–N angle.

(vii) Recently, the groups of Meyer and Neese reported a detailed study extending the series of cobalt(II) complexes with $[N_4]$ coordination.[32] Theoretical considerations for these complexes showed that the largest negative *D* values for these systems can be expected for an orthogonal orientation of the two bidentate chelating ligands (i.e., a dihedral twist angle of 90°) paired with an optimal bite angle of about 82°. In addition, they concluded that the axial ZFS parameter *D* shows a significant dependence on the electronic properties of the ligand donor atoms, which can be represented by the parameters e_σ (σ-bonding) and $e_{\pi s}$ (out-of-plane π-bonding) of the angular overlap model (AOM)[32] and is consistent with earlier findings for complexes with varying donor atoms from group 15 and 16.[56,58,59]

(viii) The above results toward the dihedral twist angle δ seem to differ from observations made earlier by us for a series of cobalt(II) SIMs with $[N_2O_2]$ coordination environment given by two chelating ligands, for which it was found that for solvomorphs of complexes containing the same ligand, a decrease in δ leads to an increase in both ZFS parameters *D* and *E*.[40,41] However, this was generally accompanied by a significant increase in the $|E/D|$ ratio when δ was lowered.

(ix) Interestingly, a similar observation has been reported for a series of cobalt(II) SIMs with an $[S_4]$ coordination environment, namely the $[Co(C_3S_5)_2]^{2-}$ complex anion with different counter cations. For this series, it was found that the calculated rhombic ZFS parameter *E* increases with smaller dihedral twist angle δ. It should be noted that the *E* values were derived from theoretical calculations and verified by magnetic relaxation investigated by ac susceptibility measurements.[64]

(x) Finally, for the bis-chelate complexes with $[N_2O_2]$ coordination environment, we have already proposed in 2016 to describe the distortion of such a pseudotetrahedral coordination geometry by the so-called elongation parameter ε_T, which is given by the ratio between the average obtuse and acute angles at the cobalt(II) ion.[39] For the parameter ε_T a nearly constant ratio $|D/\varepsilon_T|$ of about 32 cm^{-1} was observed, indicating a linear correlation.

It is notable that only a relatively small number of the reported magneto-structural correlations are based on experimental data. This is due to the limited number of examples

that provide structural variations within a comparable parameter range. Furthermore, it is widely acknowledged that accurately determining ZFS parameters from magnetometry data is a challenging endeavor, and in some cases, may not be feasible.[65–67] To address this challenge, spectroscopic techniques have been employed to facilitate direct measurement of magnetic transitions in molecular systems within the THz range.[68–71] In this context, frequency-domain Fourier-transform THz-EPR (FD-FT THz-EPR) spectroscopy has proven to be a versatile tool for a precise determination of the ZFS energy and related parameters.[72–74]

With the present study, we intend to enlarge the number of cobalt(II) SIMs for which the ZFS parameters are precisely determined in order to broaden the basis for the investigation of magneto-structural correlations. We chose the group of pseudotetrahedral cobalt(II) complexes with bis-chelate coordination and $[N_2O_2]$ donor set, as this is a subset of complexes with the largest known number of examples characterized by FD-FT THz-EPR and is easily modified by variation of the Schiff-base ligand system.[39–42] To this end, four new complexes were synthesized and fully characterized including FD-FT THz-EPR for the direct measurement of their spin-reversal barrier. The data obtained was used to explore magneto-structural correlations for the group of bis-chelate cobalt(II) complexes.

Results and Discussion

Syntheses

The four new ligands depicted in Scheme 2 were obtained in good yields by Schiff-base condensation of salicylaldehyde with para-substituted aniline derivatives (for more details see Section S1 in Supporting Information). To obtain the related complexes **1–4**, the appropriate ligand and cobalt(II) acetate tetrahydrate were reacted in a ratio of 2 : 1 at room temperature in either methanol/acetone (1 : 1, **1**), methanol (**2** and **3**) or methanol/dichloromethane (1 : 1, **4**). Single crystals suitable for X-ray diffraction were obtained by slow evaporation of the solvents.

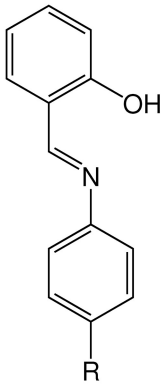

Ligand	R	$[Co(L^n)_2]$
HL^1	NMe_2	**1**
HL^2	H	**2**
HL^3	Me	**3**
HL^4	NO_2	**4**

Scheme 2. Ligands used for the synthesis of compounds **1–4**.

Crystal Structure Description

Single-crystal X-ray diffraction measurements showed that the complexes **1** and **2** crystallize in the triclinic space group $P\bar{1}$, while **3** and **4** crystallize in the monoclinic space group $C2/c$. The crystallographic data and structure refinement parameters for **1–4** are summarized in Tables S1 and S2. The investigated complexes are all neutral and mononuclear, with the cobalt(II) ion coordinated by two monoanionic chelating ligands leading to a distorted pseudotetrahedral $[N_2O_2]$ coordination environment. As an example, the molecular structure of **2** is depicted in Figure 1 (for **1**, **3**, and **4** see Figures S1–S3), selected bond lengths and angles for all complexes **1–4** are given in Table S3. The crystal structure of complex **1** contains two crystallographically independent complex molecules denoted as **1-Co1** and **1-Co2** (Figure S1). Due to a higher symmetric space group, the coordinated ligands at the cobalt(II) ion of complexes **3** and **4** are crystallographically equivalent, related by a C_2 axis (Figures S2 and S3).

All complexes exhibit a rather similar coordination environment in terms of Co–N/O bond lengths and bite angles. Hence, the bond lengths only deviate by about 1 pm (Co–N: 199.3–200.4 pm; Co–O: 189.9–191.1 pm) and the corresponding bite angles by less than 2° (95.6–97.5°). The other angles in the coordination environment of the cobalt(II) ions of **1–4** show a significant variation of more than 10° (Table S3). Nevertheless, the observed bond distances and angles are all within the expected range for complexes containing such a bidentate ligand system with [NO] donor set.[39–41,75,76]

For bis-chelate cobalt(II) complexes with a pseudotetrahedral coordination, various possible distortions have been described in Refs. [39,40,42], which are depicted in Figure 2. The well-established continuous shape measures (CShM) provide a structural descriptor $S(G)$ ($0 \leq S(G) \leq 100$; the lower limit represents the exact structure) that can be used to probe how close a molecular structure is to an ideal reference polyhedron.[77] In the case of interest here, the parameter $S(T_d)$ describes the deviation from an ideal tetrahedron.[78] For the complexes **1–4**, low values in the range from 1.28 to 1.85 are

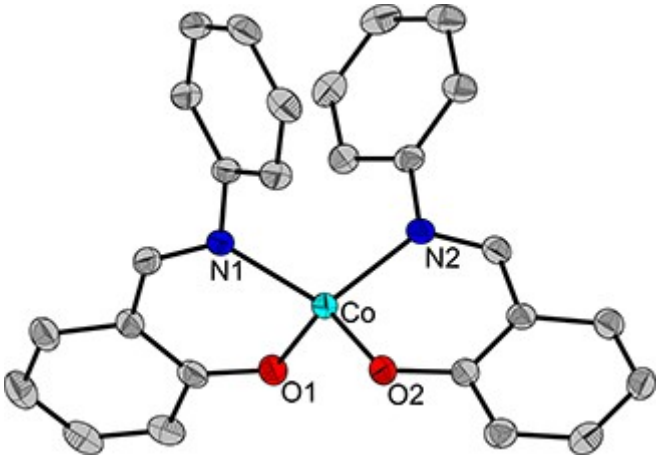

Figure 1. Molecular structure of **2**. Thermal ellipsoids are drawn at the 50% probability level and hydrogen atoms are omitted for clarity.

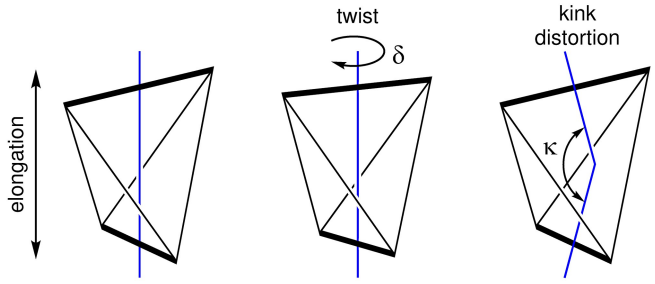

Figure 2. Perspective view of possible distortions of the pseudotetrahedral coordination geometry of bis-chelate complexes related to the (pseudo-)S_4 axis (blue): elongation, twist, and kink distortion.

observed Table 1), indicating only small distortions (values for other polyhedra are listed in Table S4). It is noteworthy that the extremes of the observed distortions are given by the two crystallographically independent molecules **1-Co1** and **1-Co2** in the crystal structure of **1** (Figure S1).

Nevertheless, the shape parameter $S(T_d)$ does not allow to discriminate the possible types of distortion sketched in Figure 2. For the twist distortion, this can be described by the dihedral angle δ between the chelate planes of the two bidentate ligands, while the kink distortion is represented by the angle κ between the two vectors given by the cobalt ion and the centroids of the two chelate planes (Table 1). For complexes **1**–**4**, the dihedral angle δ deviates slightly from 90°, the value for an ideal tetrahedron, and varies between about 79 and 86°. In accordance with the low overall distortion, the angle κ also varies in a narrow range from about 174 to 178°, which is still close to a linear arrangement of the two chelate vectors.

The third type of distortion is the elongation of the tetrahedron along the pseudo-S_4 axis of the bis-chelate coordination environment at the cobalt(II) ion, which can be measured by the parameter ε_T, the ratio between the average obtuse and acute angles (Figure 3).[39] A value of $\varepsilon_T = 1$ represents an ideal tetrahedron, while for a virtually linear molecule $\varepsilon_T \rightarrow \infty$. For **1**–**4**, the ε_T values vary between 1.19 and 1.22, which is slightly smaller than the values observed for comparable cobalt(II) complexes with sterically more demanding ligands or additional co-crystallized solvent molecules (1.24–1.28).[39–41]

All complexes show intermolecular interactions in their crystal structures (Figures S4–S13). However, there are significant variations in the packing due to the differences in their space group symmetries. In **1**, the intermolecular contacts are dominated by CH···π and NH···π interactions, leading to Co···Co distances in the range of 795 to 966 pm (Figures S4–S6). The situation is different for complex **2**, where the intermolecular π···π contacts dominate, resulting in chains along the crystallographic [101] direction with alternating Co···Co distances of 737 and 1144 pm (Figure S7), with comparatively shorter Co···Co distances of 562 pm observed between non-interacting complexes of neighboring chains. In the two remaining complexes **3** and **4**, the higher symmetry leads to a different packing situation, which is similar for both complexes and again dominated by π···π interactions (Figures S8–S11). The shortest Co···Co distances for the complexes **3** and **4** with 594 and 604 pm, respectively, are observed for contacts between complexes arranged along the crystallographic [001] axis (Figures S8 and S10). The resulting chains are further linked by additional π···π interactions, resulting in a two-dimensional arrangement along the crystallographic (100) plane with, however, significantly larger Co···Co distances in the [010] direction of 847 and 830 pm for **3** and **4**, respectively. These planar arrangements are further associated via CH···π interactions (Figures S12 and S13).

Table 1. Distortion parameters for the structures of **1**–**4** (see Figures 2 and 3).

	1-Co1	1-Co2	2	3	4
$S(T_d)$	1.85	1.28	1.55	1.67	1.83
δ/deg	81.4	85.5	85.5	79.2	79.4
κ/deg	173.8	177.7	176.5	176.5	176.1
ε_T	1.220	1.191	1.219	1.191	1.206
$\bar{\alpha}_{ob}$/deg	116.8	115.9	116.7	116.0	118.7
$\bar{\alpha}_{ac}$/deg	95.8	97.3	95.8	97.4	96.6

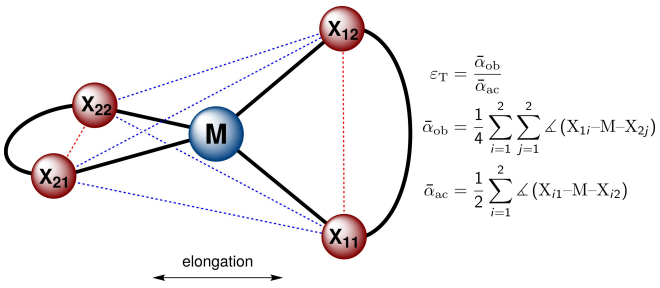

Figure 3. Definition of the elongation parameter ε_T for a bis-chelate metal complex with distorted tetrahedral [MX_4] coordination environment. Dashed lines indicate the edges of the tetrahedron related to bond angles (bite angle in red and non-bridged edges in blue).

Quantum Chemical Studies

Computational studies based on high-level *ab initio* calculations at the CASSCF/CASPT2/RASSI-SO level (see Supporting Information, Section S1.6) were performed using the molecular geometries obtained from the crystallographic data to gain first insights into the magnetochemical properties of the complexes **1**–**4**. This particularly allows to specifically address the properties of each of the symmetry-independent complex molecules present in the crystal structure of **1**. A high-spin d^7 configuration was obtained as the ground state for all complex molecules and the lowest low-spin state is well separated from the ^{4}F ground multiplet (relative CASPT2 energies for the lowest doublet state: **1-Co1** 14130 cm^{-1}; **1-Co2**: 14788 cm^{-1}; **2**: 14117 cm^{-1}; **3**: 14115 cm^{-1}; **4**: 14021 cm^{-1}). For a (pseudo-)tetrahedral coordination environment, the ^{4}F ground multiplet splits into three multiplets ($^4A_2$, $^4T_2$, and $^4T_1$), where $^4A_2$ is expected to be the

ground state term,[79] which is confirmed by the calculations in case of **1**–**4**. For the investigated compounds, the lowest $^4T_2$ and $^4T_1$ states can be found at 2370–2720 cm^{-1} and 8181–8787 cm^{-1}, respectively (see Tables S5 and S6 for CASSCF and CASPT2 energies, respectively).

Since all $^4T_1$ and $^4T_2$ states are at significantly higher energy, the magnetic properties up to room temperature can be represented primarily by the properties of the $^4A_2$ multiplet, which consists of two Kramers doublets as illustrated in Figure 4 for an easy-axis type of magnetic anisotropy ($D<0$). The corresponding energies of the spin–orbit coupled Kramers doublets can be found in Table S7 and show a ZFS in the range from 46 to 53 cm^{-1} for the $^4A_2$ term. These two Kramers doublets can be represented by an effective $S=3/2$ spin model,[80,81] for which Table 2 lists the calculated ZFS parameters D and E. For all complex molecules investigated, an easy-axis type of magnetic anisotropy ($D<0$) is obtained with calculated D values in the range from −26.7 to −23.0 cm^{-1}, for which the anisotropy axes are depicted in Figures S14 and S15. The easy axis is nearly in-plane with the two six-membered chelate rings and intersects the O–Co–N angles unevenly. Interestingly, the D values of the two symmetry-independent molecules in the crystal structure of complex **1** are close to the limits of the observed range at −26.2 (**1-Co1**) and −23.7 cm^{-1} (**1-Co2**). In general, the calculated **g** tensor shows a distinct easy axis of magnetization ($g_z > g_{x,y}$). The corresponding isotropic g_{av} values ($g_{av} = (g_x + g_y + g_z)/3$) are nearly identical (2.25–2.27). Furthermore, the magnitude of g_{av} indicates only a small orbit contribution, as expected for (pseudo-)tetrahedral cobalt(II) complexes due to the $^4A_2$ ground multiplet.

For an effective model with a pseudo-spin of $S' = 1/2$,[80,81] the corresponding g' factors representing the individual Kramers doublets are given in Table S8. The ground state Kramers doublet exhibits an almost ideal Ising case for all complex molecules in **1**–**4**, in which the magnetic easy axis g'_z coincides with the main magnetic anisotropy axis. However, in the first excited Kramers doublet, an easy plane of magnetization is apparent ($g'_{x,y} > g'_z$), for which the hard axis of magnetization (g'_z) coincides with the main magnetic anisotropy axis.

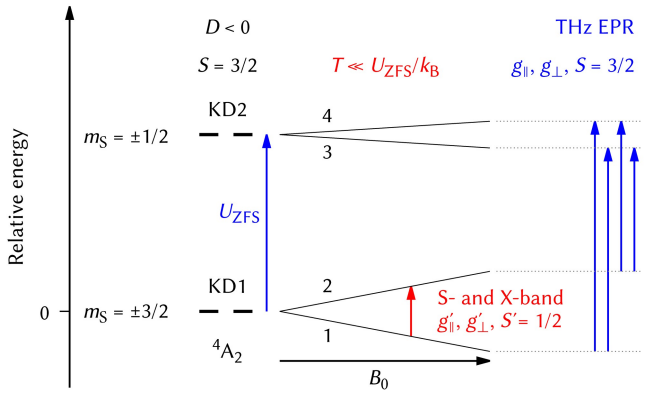

Figure 4. Energy diagram and magnetic field dependence for the $^4A_2$ ground state multiplet of a cobalt(II) ion, representing the ZFS of the two Kramers doublets (KD1 and KD2) and the possible EPR transitions and corresponding parameters (red: S- and X-band CW EPR; blue: THz EPR).

Table 2. Calculated zero-field splitting parameters D and E of the $^4A_2$ ground multiplet ($S=3/2$) as well as the corresponding main components of the **g** tensor obtained by CASSCF/CASPT2.

	1-Co1	1-Co2	2	3	4
D/cm^{-1}	−26.2	−23.7	−26.7	−23.0	−25.4
E/cm^{-1}	−1.2	−0.8	−0.7	−0.4	−0.9
E/D	0.05	0.03	0.03	0.02	0.03
g_x	2.13	2.13	2.14	2.13	2.12
g_y	2.17	2.16	2.15	2.17	2.17
g_z	2.49	2.45	2.48	2.45	2.47
g_{av}	2.27	2.25	2.26	2.25	2.25

EPR Spectroscopy

In order to experimentally address the ZFS of the complexes **1**–**4**, which is relevant for the interpretation of their magnetic properties, the compounds were studied by low temperature continuous-wave (CW) EPR and FD-FT THz-EPR experiments. The latter spectroscopic method enables a direct measurement of the energy difference between the two Kramers doublets of the $^4A_2$ ground state multiplet, which is described by the ZFS, modeled with the parameters D and E, and further denoted as U_{ZFS}. Figure 4 illustrates the case of an easy-axis type of magnetic anisotropy ($D<0$), as predicted by the quantum chemical calculations and confirmed by the S- and X-band EPR data (see below). Moreover, this energy difference also determines the magnetic-anisotropy barrier of the Orbach process, which contributes to the relaxation of the magnetization in the case of (pseudo-)tetrahedral cobalt(II) SIMs.

The results of FD-FT THz-EPR experiments for the compounds **1**–**4** performed on pressed powdered pellets at 5 K and fields up to 7.5 T are depicted in Figure 5 as relative transmittance magnetic-field division spectra (MDS). The MDS show transitions corresponding to U_{ZFS} values ranging from 39.6 to 46.5 cm^{-1} at $B_0=0$ (**1**: 39.6 and 45.7 cm^{-1}; **2**: 46.5 cm^{-1}; **3**: 41.1 cm^{-1}; **4**: 44.8 cm^{-1}). Most notably, two distinct signals can be identified in the spectra of **1**, which is consistent with the presence of two symmetry-independent complex molecules in its crystal structure (see Section "Crystal Structure Description"). Due to the significant difference in the ZFS energies for the two symmetry-independent molecules in **1** and the agreement of the experimental and theoretical values obtained by the quantum chemical *ab initio* calculations (see Section "Quantum Chemical Studies"), an assignment of the two measured energies U_{ZFS} to the individual molecular species can be successfully made (**1-Co1**: 45.7 cm^{-1}; **1-Co2** 39.6 cm^{-1}). The observed signals in the MDS are field-dependent and shift with increasing magnetic field due to the Zeeman splitting, which is governed by their respective g factors. The most intense signals, which shift to higher energies as the magnetic field increases, correspond to the excitations originating from the ground state (1 → 3 and 1 → 4; see Figure 4). In general, the magnetic-field

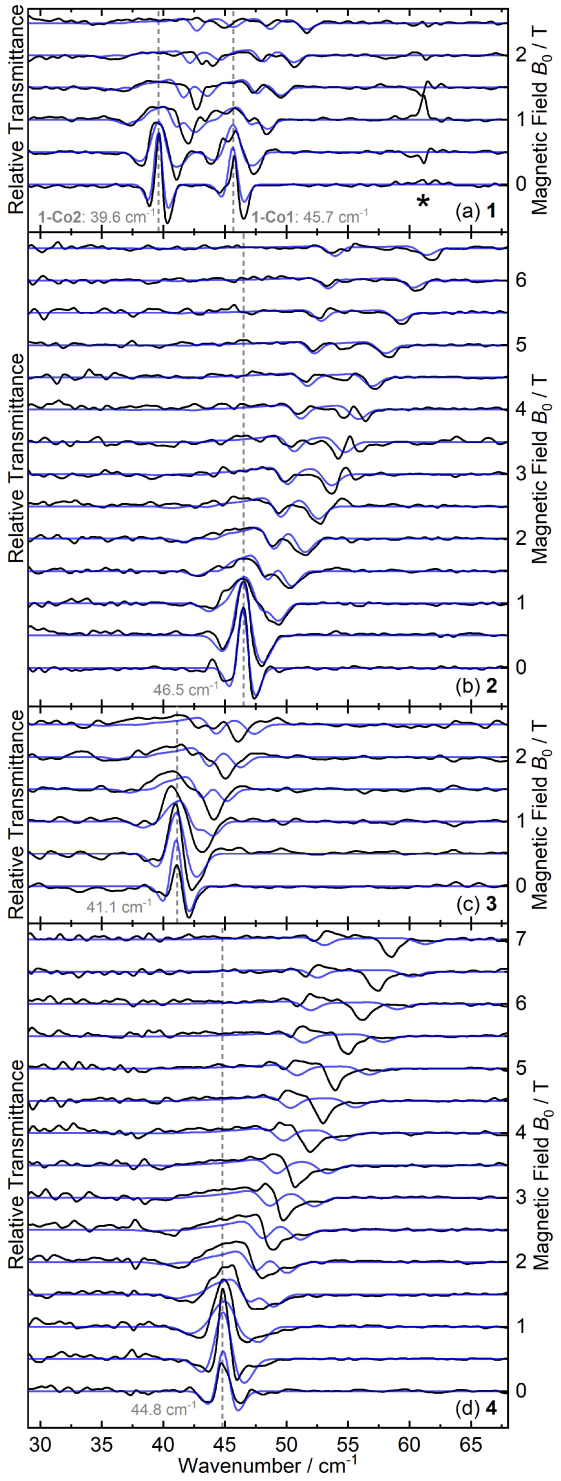

Figure 5. Experimental (black lines) and simulated (blue lines) field-dependency of the FD-FT THz-EPR spectra of **1** (a), **2** (b), **3** (c), and **4** (d) measured at 5 K. The grey dashed lines represent magnetic transitions at $B_0 = 0$. In the relative transmittance MDS, which are obtained by division of a raw spectrum at $B_0 + 0.5$ T by one measured at B_0, maxima correspond to stronger absorption at lower B_0, minima to increased absorption at higher B_0. The asterisk in (a) denotes the position of an intense vibrational transition causing artifacts in the MDS.

dependence of the observed signals in the MDS is directly correlated to the anisotropic g factors (cf. Table 2). However, it should be noted that the FD-FT THz-EPR data are most sensitive to U_{ZFS} (i.e., $2\sqrt{D^2 + 3E^2}$ for $S = 3/2$) and to a lesser extent to the individual components of the **g** tensor, while CW EPR data in the S- or X-band are particularly sensitive to the ratio $|E/D|$.[82]

Therefore, we performed additional S- and X-band CW EPR experiments on polycrystalline powder samples of **1**–**4**. Figure 6 depicts the CW EPR spectra obtained for **1** and **2**, which feature the transitions within the ground Kramers doublet corresponding to its effective $g'_{\parallel}$ and $g'_{\perp}$ values at low and high fields, respectively ($S' = 1/2$; see Figure 4). All EPR signals exhibit enhanced line broadening due to intermolecular spin–spin interactions in the polycrystalline samples and no resolved ^{59}Co hyperfine splitting. For compounds **1** and **2**, the line positions in the X-band and S-band spectra correspond approximately to $g'_{\parallel}$ and $g'_{\perp}$ values of about 8 and 0.6, respectively, which is consistent with the corresponding computational results for an effective $S' = 1/2$ pseudo-spin model (Table S8). Despite the presence of two crystallographically independent molecules in the crystal structure of **1**, which can be distinguished in the THz-EPR spectra, the S- and X-band EPR spectra of **1** can be solely described by only one set of g' transitions that

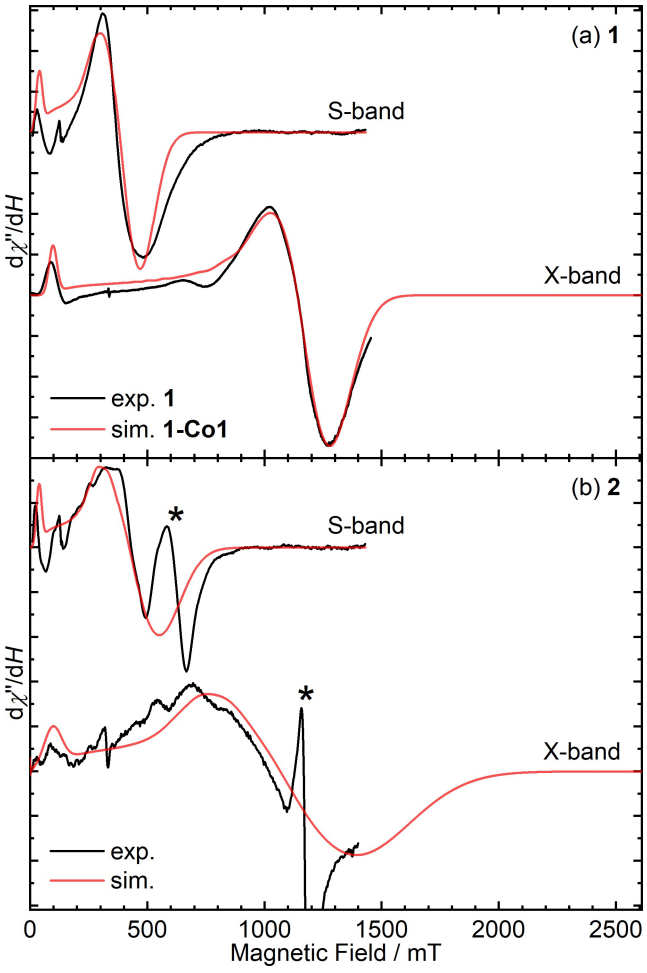

Figure 6. Experimental (black lines) and simulated (red lines) S- and X-band EPR spectra at 5 K of **1** (a) and **2** (b). Detailed experimental conditions can be found in the Supporting Information, Section S1.4. The asterisk in (b) indicates a contaminative signal from condensed $^3O_2$.

corresponds to those of **1-Co1**. This can be rationalized by the considerably smaller rhombicity $|E/D|$ of **1-Co2** (Figure S16), as evident from the quantum chemical calculations (Table 2). For the complexes **3** and **4**, only much less intense $g_{\parallel}^{'}$ peaks were observed and no $g_{\perp}^{'}$ lines could be identified within the accessible field range up to ~1.5 T, neither with X- nor S-band EPR. The very low intensity can be attributed to the very small $|E/D|$ ratios (cf. Table 2), indicative for almost pure m_S states, leading to very low EPR transition probabilities within the ground state. Furthermore, this also results in rather small $g_{\perp}^{'}$ values, which correspond to fields outside the accessible range, similar to what is observed for the case of **1-Co2** (Figure S16). In addition, the possible line broadening due to antiferromagnetic intermolecular interactions, which is evident for **3** and **4** from the susceptibility data (see Section "Static Magnetic Properties"), further complicates the detection of signals in the CW EPR spectra.

For all compounds, fits were performed according to the Hamilton given in Equation (1) using an effective $S=3/2$ spin model for the entire set of THz-EPR data and, where available, simultaneously for the corresponding CW EPR data.

$$\hat{H} = \underbrace{\mu_B \vec{B}_0 \mathbf{g} \hat{S}}_{\hat{H}_{Zeeman}} + \underbrace{D\left[\hat{S}_z^2 - \frac{1}{3}S(S+1)\right] + E\left[\hat{S}_x^2 - \hat{S}_y^2\right]}_{\hat{H}_{ZFS}} \quad (1)$$

The Hamiltonian consists of terms for the Zeeman interaction ($\hat{H}_{Zeeman}$) and the zero field splitting (ZFS; $\hat{H}_{ZFS}$), where μ_B is the Bohr magneton, $\vec{B}_0$ is the external magnetic field, **g** is the **g** tensor, $\hat{S}$ is the spin operator ($S=3/2$), and D and E are the axial and rhombic ZFS parameters, respectively. In the data analysis performed here, the **g** tensor was represented as an axial system ($g_{\parallel}$ and $g_{\perp}$). The optimized parameters of the spin Hamiltonian in Equation (1) derived from least-squares fit for **1**–**4** are summarized in Table 3 and the corresponding spectra are shown in Figures 5 and 6. These fits resulted in values of −19.8 to −23.0 cm^{-1} for the axial ZFS parameter D of the compounds **1**–**4**, which are within the expected range for pseudotetrahedral cobalt(II) complexes with an $[N_2O_2]$ donor set[39–41] and are consistent with an easy-axis type of magnetic anisotropy ($D<0$) in the ground state, the latter being preferred for the design of SIMs. In addition, the experimental values agree well with those obtained from quantum chemical *ab initio* calculations, although a slight overestimation of about 3 to 4 cm^{-1} can be observed for the latter (Table 2).

Table 3. Zero-field splitting parameters D and $|E|$ and principal components of the **g** tensor determined from simulations of the EPR data.

	1-Co1[a]	1-Co2	2[a]	3	4
D/cm^{-1}	−22.6	−19.8	−23.0	−20.5	−22.4
$\|E\|/cm^{-1}$	2.0–2.2	0.6	1.9	0.4	0.7
$\|E/D\|$	0.09–0.10	0.03[b]	0.08	0.02[b]	0.03[b]
$g_{\parallel}$	2.32	2.38[c]	2.36	2.42[c]	2.43[c]
$g_{\perp}$	2.06	2.08[c]	2.11	2.09[c]	2.08[c]
g_{av}	2.14	2.18[c]	2.19	2.20[c]	2.20[c]

[a] The strains in D and E used in the simulation of the line shapes of the CW EPR signals are as follows (in cm^{-1}): **1-Co1** 0.36 (X-band, THz-EPR), 0.76 (S-band); **2** 0.84. [b] Fixed at the values from quantum chemical *ab initio* calculations (Table 2), as no CW EPR signals could be used in the simulations. [c] Since the effective g values apparent in the THz-EPR data are affected by significant intermolecular interactions and/or spin–phonon couplings, the isotropic g_{av} value was fixed to that from dc magnetometry (cf. Table 4) and the relative axial anisotropy $(g_{\parallel}-g_{\perp})/g_{av}$ was fixed to the value resulting from the tensor components from the quantum chemical *ab initio* calculations (Table 2).

However, it should be noted here that significant differences in the agreement of simulated and experimental THz-EPR spectra are observed for the four compounds. While the simulations for **1** and **2** show excellent agreement with the experimental spectra, apart from some spin–phonon effects in the case of **1**, the THz-EPR spectra of compounds **3** and **4** show considerable deviations at higher magnetic fields. In the case of the complex species **1-Co1** and **2**, a simultaneous fit of THz-EPR and CW EPR data was possible and allowed to directly determine the rhombic ZFS parameter $|E|$ for these two complex species, revealing a moderate rhombicity of the magnetic anisotropy as represented by the $|E/D|$ ratio (**1-Co1**: 0.09–0.10; **2**: 0.08). The situation is different for the complex species **1-Co2**, **3**, and **4**, as no CW EPR data were available for a simultaneous fit, so that a different approach had to be chosen. For the latter cases, the corresponding g_{av} parameters were fixed to the values obtained from dc magnetometry (see Section "Static Magnetic Properties") and their respective $|E/D|$ ratios as well as the relative axial g anisotropies, i.e., $(g_{\parallel}-g_{\perp})/g_{av}$, have been set to the values obtained from *ab initio* calculations (see Table 2). The hereby obtained data set for **1-Co2** further corroborates the assignment made for the CW EPR spectrum of compound **1**, namely that the observed signals correspond to the complex species **1-Co1** and that no signature for the second species **1-Co2** could be found in the CW EPR spectrum. In fact, the $g^{'}$ values for an effective $S^{'}=1/2$ pseudo-spin system, relevant in the CW EPR spectra, can be predicted by projecting the g, D, and E values of the effective $S=3/2$ system (Table 3),[83–85] leading to a $g_x^{'} \simeq g_y^{'} \simeq g_{\perp}^{'}$ value of approximately 0.1 for **1-Co2**, with the corresponding EPR transitions in the S- and X-band spectra occurring at around 2.7 and 6.7 T, respectively, which is far outside the accessible field range.

The deviations in the THz-EPR spectra of compounds **3** and **4** observed at higher magnetic fields clearly indicate that lower effective g values are operative. In this context, it should be noted that it is known that such behavior can be caused by the presence of intermolecular antiferromagnetic exchange, which can be described by a mean-field approach leading to Equation (2).[86]

$$g_z^* = g_z - \frac{zJ\langle S_z\rangle}{\mu_B B_z} \quad (2)$$

The relationship given in Equation (2) shows that the effective g_z^* value, relevant for the highest energy transition in the THz-EPR spectra ($1 \rightarrow 4$; see Figure 4), is basically reduced for antiferromagnetic interactions, with the deviations decreasing as the magnetic fields increase (Figure 5). Indeed, this is

corroborated by the susceptibility data of **3** and **4**, which give clear evidence for the presence of antiferromagnetic interactions in the compounds **3** and **4** (see Section "Static Magnetic Properties"). Moreover, this is in agreement with the observed chain-like association of complex molecules in the crystal structures of **3** and **4**, which leads to rather short intermolecular Co···Co contacts (Figures S8 and S10).

In summary, FD-FT THz-EPR experiments allow a precise determination of U_{ZFS} for the complex species of the compounds **1**–**4** and even enable to discriminate between the two crystallographically independent complex molecules in **1**. However, it should be noted that g_{av} and in particular the $g_{\perp}$ component of the **g** tensors cannot be sufficiently characterized by THz-EPR spectroscopy. Thus, complementary methods such as dc magnetic susceptibility measurements are required.

Static Magnetic Properties

The magnetic susceptibility of the compounds **1**–**4** was measured between 2 and 300 K with an applied field of 0.2 T (Figure 7). At room temperature, the $\chi_M T$ values vary between 2.24 and 2.33 $cm^3 K mol^{-1}$ and are higher than the theoretical spin-only value of 1.875 $cm^3 K mol^{-1}$ for an $S = 3/2$ system,[65] indicating contributions from unquenched orbital angular momentum, a behavior well-known for pseudotetrahedral cobalt(II) complexes.[38–41,79] As expected, the $\chi_M T$ values are almost constant for all compounds **1**–**4** in the range between 50 and 300 K. Below 50 K, a sharp decrease in the $\chi_M T$ values can be observed for all compounds, which leads to a value of 1.57 $cm^3 K mol^{-1}$ at 2 K for **1** and **2**. This observation can mainly be attributed to the rather large ZFS energies U_{ZFS} as determined from the THz-EPR spectra (Table 3). Remarkably, an even stronger decrease in $\chi_M T$ can be observed for **3** and **4**, leading to values of 0.8 and 0.61 $cm^3 K mol^{-1}$, respectively. This can be attributed to significant differences in the crystal packing of the four compounds, as much shorter Co···Co distances are observed for **3** and **4** (see Figures S8 and S10), which is consistent with the presence of considerable antiferromagnetic intermolecular interactions between the molecules in the solid phase. In addition, field- and temperature-dependent magnetization measurements were also carried out for compounds **1**–**4** in the temperature range from 2 to 5 K at fields up to 5 T, whereby saturation of the magnetization was not observed in any case (Figures S17–S20). Together with the strong temperature dependence of the magnetization, this is an indication of high magnetic anisotropy. It is noteworthy that the magnetization measurements did not yield any evidence of open hysteresis loops within the range of accessible temperature and magnetic field sweep rates.[36]

Magnetic susceptibility and magnetization data for **1** and **2** were simultaneously fitted with the Hamiltonian given in Equation (1) using the program PHI.[87] In the case of complexes **3** and **4**, intermolecular interactions that occur in the crystal packing (Figures S8 and S10) had to be taken into account via a mean-field approximation. In the PHI program, however, this approximation is implemented solely for the treatment of susceptibility data. Therefore, we used a tailor-made program that is capable of simultaneously fitting magnetic susceptibility and magnetization data with the Hamiltonian provided in Equation (1) for an effective $S = 3/2$ system (for details see Supporting Information, Section S5). In these fits, the ZFS parameters for the compounds **1**–**4** were fixed to the values derived from EPR experiments, which is justified by their much higher precision.

The resulting best-fit parameters for compounds **1**–**4** are summarized in Table 4. The magnetic data could be fitted by anisotropic sets of g values for **1**–**4**, which reveals an easy-axis type of magnetic anisotropy ($g_{\parallel} > g_{\perp}$). The g_{av} values of all four compounds are similar and within the expected range for this class of compounds,[39–41] indicating the presence of spin–orbit coupling. For complexes **3** and **4**, the intermolecular interactions were approximated by mean-field theory, resulting in zJ values of −0.26 and −0.34 cm^{-1}, respectively. These values are within a reasonable range for such intermolecular magnetic interactions.[39,88]

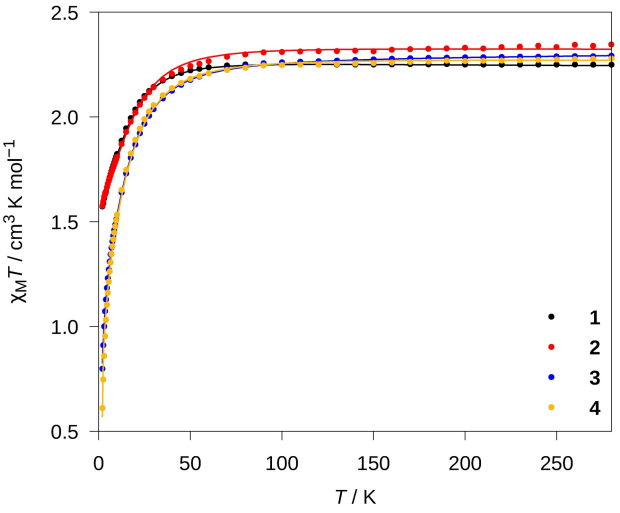

Figure 7. Temperature dependence of $\chi_M T$ for compounds **1**–**4** at an applied magnetic field of 0.2 T. The colored lines represent the best fits (**1** black, **2** red, **3** blue, **4** orange) with the parameters given in Table 4.

Table 4. Parameters determined by simultaneous least-squares fits of $\chi_M T$ and magnetization data of **1**–**4** using the Hamiltonian given in Equation (1) (for details see text).[a]

	1	2	3	4
$g_{\parallel}$	2.35	2.34	2.27	2.35
$g_{\perp}$	2.09	2.16	2.17	2.12
g_{av}	2.18	2.22	2.20	2.20
zJ/cm^{-1}	–	–	−0.26	−0.34

[a] The ZFS parameters D and $\lvert E \rvert$ were used as determined from FD-FT THz-EPR experiments (Table 3), with the average values of the species **1-Co1** and **1-Co2** used for the fitting of **1**.

Dynamic Magnetic Properties

The dynamic magnetic properties of the compounds **1**–**4** were investigated by ac susceptibility measurements with an oscillating field of 1 Oe and frequencies between 10 and 1488 Hz at various temperatures. The in-phase (χ_M') and out-of-phase (χ_M'') magnetic susceptibilities were measured in a temperature range from 2 to 6 K in steps of 0.1 K (**2** and **4**) or 0.2 K (**1** and **3**). With the exception of **2**, all complexes show field-dependent maxima for the out-of-phase susceptibility at applied dc fields of 40 and 100 mT (Figures S21–S27), whereas for **2** such a maximum could only be observed at the larger dc field of 100 mT (Figure S23). For the complexes **1**–**4**, the maxima of the out-of-phase susceptibility shift to higher temperatures with increasing frequency, which indicates a thermally controlled relaxation process. Fitting χ_M' and χ_M'' to Equation (S1) for each temperature yields a set of parameters including the isothermal (χ_0 for $\omega \rightarrow 0$) and adiabatic susceptibility (χ_S for $\omega \rightarrow \infty$) along with the relaxation time τ_c and the dispersion factor α, which represents the distribution of relaxation times. These fits were considered reliable as long as a maximum in the plot of χ_M'' vs. frequency ω was observed, resulting in the parameters summarized in Tables S9–S15 and the relevant Cole–Cole plots shown in Figures S28–S34. Moreover, the temperature dependence of the obtained relaxation times τ_c provides additional information on the contribution of the different possible magnetic relaxation processes, i.e., (i) the thermally activated Orbach process via the spin-reversal barrier (U_{Orb}), (ii) the Raman process referring to phonon-related relaxation, (iii) the direct process, and (iv) quantum tunneling of magnetization (QTM).[4,89] Based on these processes and in order to avoid over-parameterization with the available data (see Figures S35–S38), the temperature dependence of the relaxation times of **1**–**4** is described by the expression given in Equation (3).

$$\tau_c^{-1} = \tau_0^{-1} \exp\left(\frac{-U_{Orb}}{k_B T}\right) + \tau_{vib}^{-1} \exp\left(\frac{-U_{vib}}{k_B T}\right) + \tau_{QTM}^{-1} \quad (3)$$

The first term in Equation (3) describes the contribution of the Orbach process, which usually becomes the most prominent relaxation process at higher temperatures and is characterized by the ZFS of the $^4A_2$ ground multiplet (see Figure 4). The corresponding spin-reversal barrier was set to the ZFS energy U_{ZFS} obtained from the FD-FT THz-EPR experiments of the compounds **1**–**4**, and not fitted to the experimental relaxation times, due to much higher precision of the spectroscopically determined values. A second relaxation process is given by the interaction of the molecular spin with phonon modes. Due to the molecular nature of the complexes, this relaxation process can be described by an interaction *via* discrete spin–phonon coupled states, which in turn can be expressed with an exponential term, where the exponent refers to the energy of the spin–phonon coupled state.[90] It can be assumed that more than one discrete spin–phonon coupled state contributes to the magnetic relaxation. However, to avoid over-parameterization, only a single additional exponential term is used in Equation (3) to fit the data, where the energy U_{vib} can be interpreted as the weighted sum of the energies of all contributing spin–phonon coupled states below the spin-reversal barrier.

The temperature dependence of the relaxation times τ_c of the complexes **1**–**3** were fitted to Equation (3) and the parameters obtained are summarized in Table 5. The resulting Arrhenius diagrams are shown in Figures S35–S38 together with the relevant contributions of the individual relaxation processes. It can be stated that within the accessible experimental range between about 2 and 4.5 K, the Orbach process contributes most for all complexes at higher temperatures, so that the overall relaxation behavior is qualitatively rather similar. In addition, all four complexes show a significant contribution of spin–phonon related processes at intermediate temperatures. Nevertheless, the relaxation behavior of complex **4** exhibits a clear difference, as it can be followed within the largest temperature window and since for temperatures below 3 K the experimental relaxation time τ_c is apparently independent of the temperature (Figure S38). The latter indicates quantum tunneling of magnetization, which shows the expected field dependence and was not observed for the other complexes in their respective experimentally accessible temperature range.

Table 5. Magnetic relaxation parameters of complexes **1**–**4** obtained by fitting the experimental relaxation times τ_c to Equation (3).

	B_0/mT	U_{Orb}[a]/cm^{-1}	τ_0/10^{-10} s	U_{vib}/cm^{-1}	τ_{vib}/10^{-6} s	τ_{QTM}/10^{-3} s
1	40	42.6[b]	1.24	27.3	0.097	–
	100	42.6[b]	1.90	29.0	0.055	–
2	100	46.5	0.56	11.3	49.98	–
3	40	41.1	0.71	15.8	7.540	–
	100	41.1	0.72	10.2	111.98	–
4	40	44.8	0.55[c]	34.8	0.178	3.03
	100	44.8	0.55[c]	41.2	0.062	4.49

[a] U_{Orb} is fixed to the values U_{ZFS} determined from FD-FT THz-EPR spectra (Table 3). [b] Average value of the species **1-Co1** and **1-Co2**. [c] The value for τ_0 was adjusted to produce an approximately asymptotic line for the Orbach contribution at the data point at the highest temperature; this time constant can therefore be regarded as a lower limit.

Magneto-Structural Correlations

The data available in the literature on cobalt(II)-based SIMs for magneto-structural correlations are rather scarce and often suffer from a lack of sufficient accuracy as far as the energy barriers for spin reversal are concerned. From the large number of cobalt(II) complexes with SIM behavior reported in the literature, we focus on pseudotetrahedral examples with a bis-chelate coordination, as this restriction reduces the possible structural variations. In this context, a series of complexes with $[N_2O_2]$ and $[N_4]$ donor sets at the cobalt(II) ion have been reported in the literature, which are listed in Tables S16 and S17, respectively. In order to establish reliable magneto-structural correlations, precise knowledge of the magnetic and structural parameters is a prerequisite. The corresponding data sets of cobalt(II) complexes with $[N_2O_2]$ and $[N_4]$ donor sets for which the ZFS energy U_{ZFS} could be determined using spectroscopic methods are summarized in Table 6.

It has been proposed that the bite angle of the chelate ligands should be a decisive parameter for the size of the axial ZFS parameter *D*.[29,30,32] This was essentially based on theoretical considerations in which the electronic properties of the ligand donor atoms were additionally taken into account.[32] In this context, it should be noted that the electronic properties of the donor atoms for the two cases of $[N_2O_2]$ and $[N_4]$ donor sets at the cobalt(II) ions are substantially different in terms of π contributions, *i.e.*, in the complexes **1**–**4** the oxygen atom is a π-donor, whereas the nitrogen atom is a weak π-acceptor (for AOM parameters see Table S18). In addition, the bite angles of the bis-chelate complexes are mainly determined by the rigid ligand backbone, so that only a small variation is observed within the available complex series from Table 6 ($[N_2O_2]$: 93.0–97.4° and $[N_4]$: 80.4–80.7°). Therefore, a simple common quantitative correlation for compounds from both groups of donor sets cannot be derived.

However, the situation is different when it comes to more general parameters that describe the possible distortions of a tetrahedral coordination environment of bis-chelate complexes (cf. Figure 2). In this context, the twist distortion can be described by the dihedral angle δ between the chelate planes of the two bidentate ligands, whereas the kink distortion is characterized by the angle κ between the two vectors given by the cobalt ion and the centroids of the two chelate planes, where an ideal tetrahedron is characterized by the values 90 and 180° for δ and κ, respectively. The corresponding deviations from an ideal tetrahedron can thus be described as $90°-\delta$ for the dihedral twist and $180°-\kappa$ for the kink distortion. Finally, perhaps the most fundamental form of distortion in bis-chelate complexes is the elongation of the tetrahedron, which is largely determined by the bite angle, but as such cannot be sufficiently described by this parameter alone. To provide a sufficient definition, we introduced the so-called elongation parameter ε_T,[39] which is based on the full set of angles of the first coordination sphere of the cobalt(II) ion, i.e., the ratio between the average obtuse and acute angles, to describe the degree of elongation in a tetrahedron (Figure 3). In principle, the range for ε_T is given with the lower limit for an ideal tetrahedron ($\varepsilon_T = 1$), while ε_T goes to infinity for a virtual linear molecule ($\varepsilon_T \rightarrow \infty$).

For bis-chelate complexes with $[N_2O_2]$ coordination environment, similar to those studied here, it was found that the axial ZFS parameter *D* can be projected onto the elongation

Table 6. Structural and magnetic parameters of cobalt(II) complexes with $[N_2O_2]$ and $[N_4]$ donor environment, for which the ZFS energy U_{ZFS} was determined by spectroscopic methods. The parameters that describe the structural variations are the bite angle β, the elongation ε_T, the dihedral twist angle of the chelate planes δ, and the kink distortion given by the angle κ (see text for details). The formal charge of the ligands is given for their deprotonated coordinating form.

Entry[a]	Compound in Ref.	Donor set	Ligand charge	β/deg	ε_T	δ/deg	$(180°-\kappa)$/deg	D/cm^{-1}	$\lvert E/D \rvert$	U_{ZFS}/cm^{-1}	Ref.
1	**1-Co1**	$[N_2O_2]$	−1	95.8	1.220	81.4	6.2	−22.6	0.093	45.7	this work
2	**1-Co2**	$[N_2O_2]$	−1	97.3	1.191	85.5	2.3	−19.8	0.030[b]	39.6	
3	**2**	$[N_2O_2]$	−1	95.8	1.219	85.5	3.5	−23.0	0.083	46.5	
4	**3**	$[N_2O_2]$	−1	97.4	1.191	79.2	3.5	−20.5	0.020[b]	41.1	
5	**4**	$[N_2O_2]$	−1	96.6	1.206	79.4	3.9	−22.4	0.031[b]	44.8	
6	**1**	$[N_2O_2]$	−1	94.8	1.242	72.4	5.6	−23.1	0.126	47.3	[40,41]
7	**1**·2MeOH	$[N_2O_2]$	−1	94.6	1.260	55.9	1.9	−26.8	0.142	55.3	[41]
8	**2**	$[N_2O_2]$	−1	93.0	1.283	65.3	2.2	−30.6	0.134	62.8	[40,41]
9	**2**·CH_2Cl_2	$[N_2O_2]$	−1	93.5	1.260	78.8	6.9	−25.1	0.072[c]	50.6	[39,41]
10	**1**	$[N_2O_2]$	−1	94.9	1.229	88.9	16.8	−29.5	–	58.9	[42]
32	**1**	$[N_4]$	−2	80.6	1.557	85.0	2.6	−115	–	230	[27]
33	**KCoA**	$[N_4]$	−2	80.6[d]	1.559[d]	85.2[d]	4.7[d]	−118	–	236	[31]

[a] The numbers refer to the entries of Tables S16 and S17. [b] Fixed values from quantum chemical *ab initio* calculations (Table 2), as no CW EPR data was available (see Table 3). [c] No CW EPR data were available to support the determination of the rhombicity, therefore this value is subject to considerable uncertainty. [d] Average value for two independent molecules in the crystal structure (see Table S17).

parameter ε_T leading to an almost constant ratio of $|D/\varepsilon_T|$ of about 32 cm^{-1}.[39] By scaling with the formal charge q of the coordinating chelate ligand this relationship could even be extended to cobalt(II) complexes with $[N_4]$ coordination environment. This indicates a linear dependency between the ZFS energy, the latter being mainly determined by the axial component D, and the elongation parameter ε_T. If we consider that ε_T has the value 1 for an ideal tetrahedron and that a linear scaling by the formal ligand charge applies, we can derive the linear expression in Equation (4).

$$U_{ZFS} = m_\varepsilon(\varepsilon_T - 1)|q| \quad (4)$$

Fitting all available data points summarized in Table 6 to Equation (4), with the exception of entry 10, which corresponds to an example with a large kink distortion, results in a slope of $m_\varepsilon = 209$ cm^{-1} (entry 1 in Table S19); a graphical representation is depicted in Figure 8. Using a general slope-intercept form for the linear correlation as in Equation (S4), the fit for the relevant data points confirms the assumed line through the origin based on the values obtained for slope and intercept (entry 2 in Table S19). As mentioned above, the electronic properties of the ligand donor atoms also influence the magnetic anisotropy, so that it cannot be assumed with certainty that the mixed donor set in the bis-chelate $[N_2O_2]$ cobalt(II) complexes leads to a vanishing ZFS energy for an ideal tetrahedral geometry. To probe this, we additionally performed fits solely for the relevant complexes with $[N_2O_2]$ donor set from Table 6 (entries 1–9) utilizing Equations (4) and (S4), which represent a line through the origin (i.e., forced vanishing anisotropy) and the general case, respectively (see entries 3 and 4 in Table S19). In both cases, the slope within the statistical error is the same as in the case where the $[N_4]$-cobalt(II) complexes are also included. Furthermore, the intercept is found to be close to zero in the general case, although in this case it should be noted that the statistical error is, as expected, extremely large due to the rather narrow range of the parameter set. Finally, Figure S39 gives an overview of the complete data set of currently known bis-chelate cobalt(II) complexes with $[N_2O_2]$ (Table S16) and $[N_4]$ (Table S17) donor set together with the correlation found for the data points summarized in Table 6 (see Figure 8). Although the same general trend is evident for the entire data set, large deviations from the magneto-structural correlation can be found for complexes for which the ZFS energy has not been determined by spectroscopic methods.

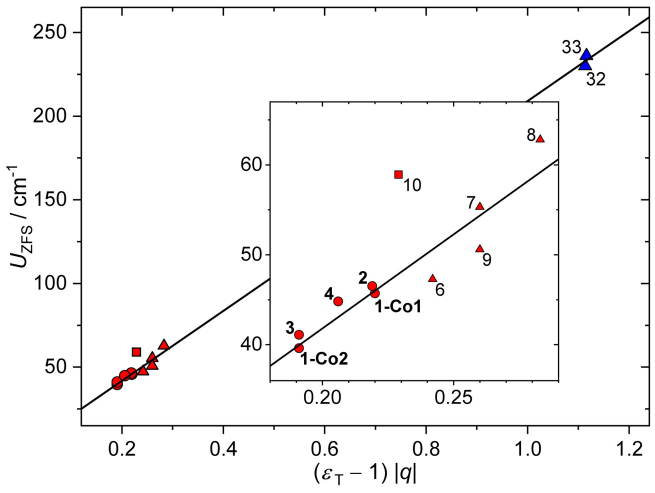

Figure 8. Correlation diagram for the ZFS energy U_{ZFS} using Equation (4) for the data points summarized in Table 6, except for entry 10. The inset expands the range for the complexes with $[N_2O_2]$ donor set. The solid line represents the fitted correlation curve. Color and symbol code: red, complexes with $[N_2O_2]$ donor set; blue, complexes with $[N_4]$ donor set; circles, complexes **1**–**4**; triangles, literature known complexes used for the fitting; square, complex with large kink distortion not used for fitting (entry 10).

To investigate previous evidence that a larger dihedral twist angle leads to increasing magnetic anisotropy for bis-chelate $[N_2O_2]$ complexes with the same coordinating ligand environment,[40,41] we performed a 2D fitting that includes the twist distortion as an additional variable with the corresponding relationship given in Equation (5).

$$U_{ZFS} = m_\varepsilon(\varepsilon_T - 1)|q| + m_\delta(90^\circ - \delta) \quad (5)$$

Here, an additional linear term describes the deviation from an ideal tetrahedron by the difference of the dihedral angle relative to 90°. The resulting 2D correlation diagram from the fitting of all data points that were also used for the previous U_{ZFS} vs. (ε_T−1) correlation (Table 6, Figure 8) is shown in Figure S40. This result shows that the dependence of the ZFS energy on the elongation parameter remains unchanged by the inclusion of the second variable, for which a slope value of zero was found (entry 5 in Table S19). Consequently, the ZFS energy U_{ZFS} of the investigated complexes can be described exclusively by the elongation parameter ε_T, as the variations in the dihedral twist angle δ are already represented by the definition of ε_T.

Irrespective of this result, however, values of δ close to the ideal dihedral angle of 90° for a tetrahedron are expected to lead to a vanishing rhombicity of the ZFS, i.e., to an $|E/D|$ ratio close to zero.[32] Moreover, for solvomorphs of bis-chelate cobalt(II) complexes, it was observed that decreasing δ values lead to an increase in the ZFS parameters D and E,[40,41] which was also accompanied by a significant increase in the rhombicity value $|E/D|$. In this context, it is also worth mentioning that the rhombic ZFS parameter E plays a crucial role, as it is associated with the occurrence of quantum tunneling of magnetization.[91]

We therefore additionally checked whether the available relevant experimental data (entries 1, 3, and 6–8 in Table 6) show a dependence on the dihedral angle. A simple approach can be implemented using the linear expression in slope-intercept form specified in Equation (6).

$$|E/D| = m_{|E/D|}(90^\circ - \delta) + b_{|E/D|} \quad (6)$$

It should be noted that such a simple approach can be considered only for cases where the donor atoms are the same within the whole series, so that additional effects due to the electronic properties of the donor atoms do not have to be taken into account. Therefore, based on the available experimental data given in Table 6, only the complexes with $[N_2O_2]$

donor set are a suitable choice. For bis-chelate $[N_2O_2]$ cobalt(II) complexes, a non-zero intercept is expected, as even for a virtually ideal tetrahedron the mixed N,O donor set should already be associated with a small rhombicity of the magnetic anisotropy. The fit obtained according to Equation (6) is depicted in Figure 9 and the relevant parameters are summarized as entry 6 in Table S19. This appears to contradict to some extent previous reports of bis-chelate $[N_4]$ cobalt(II) complexes with dihedral angles δ in the range of about 90 to 48°,[32] for which a slightly progressive increase in rhombicity $|E/D|$ was observed for decreasing values of δ, starting from $|E/D| = 0$ for the orthogonal orientation of the chelate planes ($\delta = 90°$). However, the non-vanishing rhombicity associated with the observed intercept in the linear fit of the $[N_2O_2]$ cobalt(II) complexes most likely represents the asymmetry given by the mixed nitrogen and oxygen donors, while the possible description as a linear function in this case may simply be due to a rather smooth progression, making a linear function still a reasonable approximation.

In a recent report, we have shown that, in addition to the structural parameters ε_T and δ discussed above, a so-called kink distortion (Figure 2) of the tetrahedron can also influence the ZFS energy U_{ZFS}.[42] For all bis-chelate $[N_2O_2]$ cobalt(II) complexes given in Table 6, the parameter relevant for the kink distortion ($180° - \kappa$) does not vary strongly and lies in the range from 1.9 to 6.9°, with the exception of entry 10, which has a value of 16.8°. Considering their ZFS energies, this directly implies that any term added to Equation (4) to potentially describe a contribution from this kink distortion cannot be linear. In a first simple attempt, we have therefore introduced an additional quadratic term to Equation (4) that includes a possible shift on the variable axis, which leads to Equation (7), for which two new parameters are added, namely a_κ, the curvature and κ_0, the shift of the parabola.

$$U_{ZFS} = m_\varepsilon(\varepsilon_T - 1)|q| + a_\kappa[(180° - \kappa) - \kappa_0]^2 \quad (7)$$

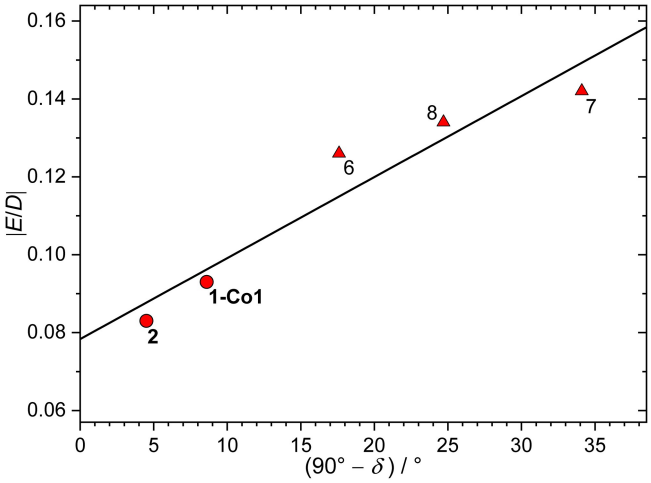

Figure 9. Correlation diagram of $|E/D|$ vs. ($90° - \delta$) for complexes with spectroscopically determined values from Table 6 (entries 1, 3, and 6–8). For color and symbol code see legend of Figure 8.

The best fit of the data for the bis-chelate $[N_2O_2]$-cobalt(II) complexes from Table 6 to Equation (7) with a fixed value of 209 cm^{-1} for m_ε, as obtained from the correlation U_{ZFS} vs. ε_T, is shown in Figure S41 and the parameters obtained are summarized in Table S19 (entry 7). Although this is clearly a simplified approach based mainly on the rather strong effect observed in the example with the large distortion angle of 16.8° (entry 10 in Table 6), the result obtained indicates a progressive increase of the ZFS energy U_{ZFS} with increasing distortion and suggests a deviation of about 6° from the expected linear arrangement of an ideal tetrahedral geometry with $\kappa = 180°$ for minimum ZFS energies. However, in order to substantiate these results, further examples with a distortion at different κ angles smaller than 174° would be required, for which the corresponding spectroscopic data are currently lacking.

Conclusions

We have presented here a series of four new pseudotetrahedral cobalt(II) complexes with $[N_2O_2]$ donor set. All complexes show SIM behavior, as they exhibit a slow relaxation of magnetization under an applied static magnetic field. These complexes have been extensively characterized, including FD-FT THz-EPR spectroscopy, which allowed to accurately determine the ZFS energies (U_{ZFS}). In one of the newly investigated complexes, two symmetry-independent molecules were found in the crystal structure, which could be distinguished in FD-FT THz-EPR spectroscopy, allowing the determination of their individual U_{ZFS} values. The determination of the parameters describing the magnetic properties of the new complexes has been complemented by the combination of CW EPR spectroscopy, magnetic susceptibility, and magnetization measurements. Quantum chemical *ab initio* calculations based on multi-reference theory (CASSCF/CASPT2/RASSI-SO) confirmed these results and revealed a strong easy-axis type of magnetic anisotropy in the investigated complexes.

Together with the structural and magnetic data for a series of additional bis-chelate cobalt(II) complexes with $[N_2O_2]$ and $[N_4]$ donor environment reported in the literature, magneto-structural correlations could be established for the U_{ZFS} values given by the energy difference between the two lowest Kramers doublets. For all these compounds, U_{ZFS} could be determined directly using spectroscopic methods, which is the basis for reliable data analysis and the search for structural correlations. In general, the possible distortions of a tetrahedral coordination environment of bis-chelate complexes include the elongation of the tetrahedron, the twisting of the two chelate planes, and a so-called kink distortion, which results from a nonlinear arrangement of the chelate ligands at the cobalt(II) ion. They can be described by the elongation parameter ε_T, the dihedral twist angle δ, and the kink angle κ, respectively. It was found that the elongation parameter ε_T, scaled by the formal charge of the chelate ligand, can sufficiently describe the ZFS energy in a linear correlation for the entire series of complexes, except for one example that exhibits an exceptionally large kink distortion. Particularly noteworthy is the fact that the ε_T parameter allows

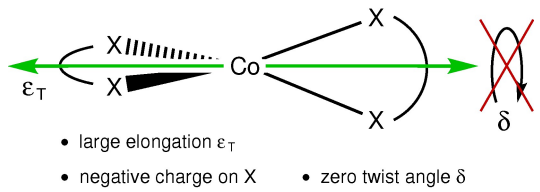

Scheme 3. Representation of the desired geometric situation for the coordination environment of four-coordinate cobalt(II) complexes leading to a large spin-reversal barrier.

to include donor environments with different sets of donor atoms in the correlation. Furthermore, the correlation of the experimental data clearly showed that the twist distortion is not a relevant parameter for the observed ZFS energy, but rather determines the rhombicity $|E/D|$ of the magnetic anisotropy of the cobalt(II) ions, so that an increasing deviation from the ideal geometry leads to an increased rhombicity.

In summary, these findings can be translated into a design principle for high-barrier tetrahedral cobalt(II) SIMs with chelating ligands. What is needed for this behavior are anionic ligands with low bite angles in combination with comparatively long bond lengths, as sketched in Scheme 3. When comparing homo- and heteroleptic cases, it is noteworthy that complexes with a homoleptic donor environment (e.g., $[N_4]$) exhibit larger barriers than complexes with a heteroleptic donor environment (e.g., $[N_2O_2]$). However, this can be attributed to the generally higher negatively charged ligands in the homoleptic cases. Therefore, it can be concluded that the effect of charged ligands is the important factor, rather than the question of a homo- or heteroleptic coordination environment. In addition, to reduce quantum tunneling effects due to rhombicity of the magnetic anisotropy, it is beneficial to reduce any twist distortion in the coordination environment.

Acknowledgements

The authors thank Dr. Axel Buchholz and Dr. Oluseun Akintola for the measurement of the magnetic data, as well as Dr. Karsten Holldack and Dirk Ponwitz for assistance with the FD-FT THz-EPR experiments. We are grateful to Prof. Atanasov for providing us the AOMX program. The purchase of ESR equipment was enabled by the Deutsche Forschungsgemeinschaft (DFG, German Research Foundation, project number INST 275/406-1 FUGG) and the state of Thuringia. We thank the HZB for the allocation of synchrotron radiation beamtime at BESSY II (Plass 222-11370 and 231-11755) and thankfully acknowledge the financial support by HZB. Open Access funding enabled and organized by Projekt DEAL.

Conflict of Interests

There are no conflicts to declare.

Data Availability Statement

The data that support the findings of this study are available in the supplementary material of this article.

Keywords: cobalt · magnetic properties · EPR spectroscopy · *ab initio* calculations · electronic structure

[1] R. Sessoli, D. Gatteschi, A. Caneschi, M. A. Novak, *Nature* **1993**, *365*, 141.
[2] M. Shiddiq, D. Komijani, Y. Duan, A. Gaita-Ariño, E. Coronado, S. Hill, *Nature* **2016**, *531*, 348.
[3] M. R. Wasielewski, M. D. E. Forbes, N. L. Frank, K. Kowalski, G. D. Scholes, J. Yuen-Zhou, M. A. Baldo, D. E. Freedman, R. H. Goldsmith, T. Goodson, M. L. Kirk, J. K. McCusker, J. P. Ogilvie, D. A. Shultz, S. Stoll, K. B. Whaley, *Nat. Chem. Rev.* **2020**, *4*, 490.
[4] D. Aravena, E. Ruiz, *Dalton Trans.* **2020**, *49*, 9916.
[5] L. Bogani, W. Wernsdorfer, *Nat. Mater.* **2008**, *7*, 179.
[6] M. Urdampilleta, S. Klyatskaya, J.-P. Cleuziou, M. Ruben, W. Wernsdorfer, *Nat. Mater.* **2011**, *10*, 502.
[7] S. Rao, J. Ashtree, A. Soncini, *Phys. Condens. Matter* **2020**, *592*, 412237.
[8] D. Gatteschi, R. Sessoli, J. Villain, *Molecular nanomagnets*, vol. 5, Oxford University Press, USA **2006**.
[9] D. Gatteschi, R. Sessoli, *Angew. Chem. Int. Ed.* **2003**, *42*, 268.
[10] A. J. Tasiopoulos, A. Vinslava, W. Wernsdorfer, K. A. Abboud, G. Christou, *Angew. Chem. Int. Ed.* **2004**, *43*, 2117.
[11] H. Oshio, M. Nakano, *Chem. Eur. J.* **2005**, *11*, 5178.
[12] A. M. Ako, I. J. Hewitt, V. Mereacre, R. Clérac, W. Wernsdorfer, C. E. Anson, A. K. Powell, *Angew. Chem. Int. Ed.* **2006**, *45*, 4926.
[13] K. S. Pedersen, J. Bendix, R. Clérac, *Chem. Commun.* **2014**, *50*, 4396.
[14] J. Ferrando-Soria, J. Vallejo, M. Castellano, J. Martínez-Lillo, E. Pardo, J. Cano, I. Castro, F. Lloret, R. Ruiz-García, M. Julve, *Coord. Chem. Rev.* **2017**, *339*, 17.
[15] J. M. Frost, K. L. M. Harriman, M. Murugesu, *Chem. Sci.* **2016**, *7*, 2470.
[16] M. Feng, M.-L. Tong, *Chem. Eur. J.* **2018**, *24*, 7574.
[17] S. T. Liddle, J. van Slageren, *Chem. Soc. Rev.* **2015**, *44*, 6655.
[18] M. Georgiev, H. Chamati, *ACS Omega* **2022**, *7*, 42664.
[19] O. Waldmann, *Inorg. Chem.* **2007**, *46*, 10035.
[20] F. Neese, D. A. Pantazis, *Faraday Discuss.* **2011**, *148*, 229.
[21] M. Murrie, *Chem. Soc. Rev.* **2010**, *39*, 1986.
[22] P. K. Sahu, R. Kharel, S. Shome, S. Goswami, S. Konar, *Coord. Chem. Rev.* **2023**, *475*, 214871.
[23] E. Carl, S. Demeshko, F. Meyer, D. Stalke, *Chem. Eur. J.* **2015**, *21*, 10109.
[24] Y.-Y. Zhu, F. Liu, J.-J. Liu, Y.-S. Meng, S.-D. Jiang, A.-L. Barra, W. Wernsdorfer, S. Gao, *Inorg. Chem.* **2016**, *56*, 697.
[25] H.-H. Cui, F. Lu, X.-T. Chen, Y.-Q. Zhang, W. Tong, Z.-L. Xue, *Inorg. Chem.* **2019**, *58*, 12555.
[26] S. K. Gupta, H. H. Nielsen, A. M. Thiel, E. A. Klahn, E. Feng, H. B. Cao, T. C. Hansen, E. Lelièvre-Berna, A. Gukasov, I. Kibalin, S. Dechert, S. Demeshko, J. Overgaard, F. Meyer, *JACS Au* **2023**, *3*, 429.
[27] Y. Rechkemmer, F. D. Breitgoff, M. van der Meer, M. Atanasov, M. Hakl, M. Orlita, P. Neugebauer, F. Neese, B. Sarkar, J. van Slageren, *Nat. Commun.* **2016**, *7*, 10467.
[28] T. Wu, Y.-Q. Zhai, Y.-F. Deng, W.-P. Chen, T. Zhang, Y.-Z. Zheng, *Dalton Trans.* **2019**, *48*, 15419.
[29] M. Wang, H.-J. Xu, T.-M. Sun, H.-H. Cui, Y.-Q. Zhang, L. Chen, Y.-F. Tang, *J. Solid State Chem.* **2021**, *299*, 122209.
[30] C. M. Legendre, E. Damgaard-Møller, J. Overgaard, D. Stalke, *Eur. J. Inorg. Chem.* **2021**, 3108.
[31] H. Bamberger, U. Albold, J. D. Midlíková, C.-Y. Su, N. Deibel, D. Hunger, P. P. Hallmen, P. Neugebauer, J. Beerhues, S. Demeshko, F. Meyer, B. Sarkar, J. van Slageren, *Ionrg. Chem.* **2021**, *60*, 2953.
[32] S. K. Gupta, S. V. Rao, S. Demeshko, S. Dechert, E. Bill, M. Atanasov, F. Neese, F. Meyer, *Chem. Sci.* **2023**, *14*, 6355.
[33] J. M. Zadrozny, J. Telser, J. R. Long, *Polyhedron* **2013**, *64*, 209.
[34] J. M. Zadrozny, J. R. Long, *J. Am. Chem. Soc.* **2011**, *133*, 20732.
[35] S. Sottini, G. Poneti, S. Ciattini, N. Levesanos, E. Ferentinos, J. Krzystek, L. Sorace, P. Kyritsis, *Inorg. Chem.* **2016**, *55*, 9537.
[36] S. Vaidya, S. Tewary, S. K. Singh, S. K. Langley, K. S. Murray, Y. Lan, W. Wernsdorfer, G. Rajaraman, M. Shanmugam, *Inorg. Chem.* **2016**, *55*, 9564.
[37] X.-N. Yao, M.-W. Yang, J. Xiong, J.-J. Liu, C. Gao, Y.-S. Meng, S.-D. Jiang, B.-W. Wang, S. Gao, *Inorg. Chem. Front.* **2017**, *4*, 701.

[38] A. Buchholz, A. O. Eseola, W. Plass, *C. R. Chim.* **2012**, *15*, 929.
[39] S. Ziegenbalg, D. Hornig, H. Görls, W. Plass, *Inorg. Chem.* **2016**, *55*, 4047.
[40] M. Böhme, S. Ziegenbalg, A. Aliabadi, A. Schnegg, H. Görls, W. Plass, *Dalton Trans.* **2018**, *47*, 10861.
[41] M. H. Pohle, M. Böhme, T. Lohmiller, S. Ziegenbalg, L. Blechschmidt, H. Görls, A. Schnegg, W. Plass, *Chem. Eur. J.* **2023**, *29*, e202202966.
[42] S. Lima, M. H. Pohle, M. Böhme, H. Görls, T. Lohmiller, A. Schnegg, R. Dinda, W. Plass, *Dalton Trans.* **2023**, *52*, 9787.
[43] P. Cucos, F. Tuna, L. Sorace, I. Matei, C. Maxim, S. Shova, R. Gheorghe, A. Caneschi, M. Hillebrand, M. Andruh, *Inorg. Chem.* **2014**, *53*, 7738.
[44] D.-K. Cao, R.-H. Wei, X.-X. Li, Y.-W. Gu, *Dalton Trans.* **2015**, *44*, 5755.
[45] A. K. Mondal, V. S. Parmar, S. Biswas, S. Konar, *Dalton Trans.* **2016**, *45*, 4548.
[46] R. Mitsuhashi, S. Hosoya, T. Suzuki, Y. Sunatsuki, H. Sakiyama, M. Mikuriya, *Dalton Trans.* **2019**, *48*, 395.
[47] R. Mitsuhashi, S. Hosoya, T. Suzuki, Y. Sunatsuki, H. Sakiyama, M. Mikuriya, *RSC Adv.* **2020**, *10*, 43472.
[48] G. Peng, Y. Chen, B. Li, Y.-Q. Zhang, X.-M. Ren, *Dalton Trans.* **2020**, *49*, 5798.
[49] Y. Chen, Q. Yang, G. Peng, Y.-Q. Zhang, X.-M. Ren, *Dalton Trans.* **2021**, *50*, 13830.
[50] W. Huang, T. Liu, D. Wu, J. Cheng, Z. Ouyang, C. Duan, *Dalton Trans.* **2013**, *42*, 15326.
[51] L. Smolko, J. Černák, M. Dušek, J. Miklovič, J. Titiš, R. Boča, *Dalton Trans.* **2015**, *44*, 17565.
[52] L. Smolko, J. Černák, J. Kuchár, C. Rajnák, J. Titiš, R. Boča, *Eur. J. Inorg. Chem.* **2017**, 3080.
[53] I. Nemec, R. Herchel, M. Kern, P. Neugebauer, J. van Slageren, Z. Trávníček, *Materials* **2017**, *10*, 249.
[54] F. Yang, Q. Zhou, Y. Zhang, G. Zeng, G. Li, Z. Shi, B. Wang, S. Feng, *Chem. Commun.* **2013**, *49*, 5289.
[55] R. Boča, J. Miklovič, J. Titiš, *Inorg. Chem.* **2014**, *53*, 2367.
[56] M. R. Saber, K. R. Dunbar, *Chem. Commun.* **2014**, *50*, 12266.
[57] S. Vaidya, S. K. Singh, P. Shukla, K. Ansari, G. Rajaraman, M. Shanmugam, *Chem. Eur. J.* **2017**, *23*, 9546.
[58] S. Vaidya, A. Upadhyay, S. K. Singh, T. Gupta, S. Tewary, S. K. Langley, J. P. S. Walsh, K. S. Murray, G. Rajaraman, M. Shanmugam, *Chem. Commun.* **2014**, *51*, 3739.
[59] E. A. Suturina, D. Maganas, E. Bill, M. Atanasov, F. Neese, *Inorg. Chem.* **2015**, *54*, 9984.
[60] D. Maganas, S. Sottini, P. Kyritsis, E. J. J. Groenen, F. Neese, *Inorg. Chem.* **2011**, *50*, 8741.
[61] M. Idešicová, J. Titiš, J. Krzystek, R. Boča, *Inorg. Chem.* **2013**, *52*, 9409.
[62] S. Vaidya, S. K. Singh, P. Shukla, K. Ansari, G. Rajaraman, M. Shanmugam, *Chem. Eur. J.* **2017**, *23*, 9546.
[63] S. Vaidya, P. Shukla, S. Tripathi, E. Rivière, T. Mallah, G. Rajaraman, M. Shanmugam, *Inorg. Chem.* **2018**, *57*, 3371.
[64] M. S. Fataftah, S. C. Coste, B. Vlaisavljevich, J. M. Zadrozny, D. E. Freedman, *Chem. Sci.* **2016**, *7*, 6160.
[65] O. Kahn, *Molecular Magnetism*, VCH Pub., Weinheim **1993**.
[66] R. Boča, *Coord. Chem. Rev.* **2004**, *248*, 757.
[67] A. A. Pavlov, J. Nehrkorn, S. V. Zubkevich, M. V. Fedin, K. Holldack, A. Schnegg, V. V. Novikov, *Inorg. Chem.* **2020**, *59*, 10746.
[68] G. C. Brackett, P. L. Richards, H. H. Wickman, *Chem. Phys. Lett.* **1970**, *6*, 75.
[69] P. M. Champion, A. J. Sievers, *J. Chem. Phys.* **1977**, *66*, 1819.
[70] K. Ray, A. Begum, T. Weyhermüller, S. Piligkos, J. van Slageren, F. Neese, K. Wieghardt, *J. Am. Chem. Soc.* **2005**, *127*, 4403.
[71] A. Schnegg, J. Behrends, K. Lips, R. Bittl, K. Holldack, *Phys. Chem. Chem. Phys.* **2009**, *11*, 6820.
[72] A. T. Hand, B. D. Watson-Sanders, Z.-L. Xue, *Dalton Trans.* **2024**, *53*, 4390.
[73] E. A. Suturina, J. Nehrkorn, J. M. Zadrozny, J. Liu, M. Atanasov, T. Weyhermüller, D. Maganas, S. Hill, A. Schnegg, E. Bill, J. R. Long, F. Neese, *Inorg. Chem.* **2017**, *56*, 3102.
[74] L. Devkota, D. J. SantaLucia, A. M. Wheaton, A. J. Pienkos, S. V. Lindeman, J. Krzystek, M. Ozerov, J. F. Berry, J. Telser, A. T. Fiedler, *Inorg. Chem.* **2023**, *62*, 5984.
[75] A. Elmali, Y. Elerman, I. Svoboda, H. Fuess, *Acta Crystallogr. Sect. C* **1996**, *52*, 553.
[76] J. L. van Wyk, S. F. Mapolie, A. Lennartson, M. Håkansson, S. Jagner, *Inorg. Chim. Acta* **2008**, *361*, 2094.
[77] M. Pinsky, D. Avnir, *Inorg. Chem.* **1998**, *37*, 5575.
[78] J. Cirera, P. Alemany, S. Alvarez, *Chem. Eur. J.* **2004**, *10*, 190.
[79] R. L. Carlin, *Science* **1985**, *227*, 1291.
[80] L. F. Chibotaru, L. Ungur, *J. Chem. Phys.* **2012**, *137*, 064112.
[81] D. Piwowarska, P. Gnutek, C. Rudowicz, *Appl. Magn. Reson.* **2019**, *50*, 797.
[82] J. Nehrkorn, I. A. Valuev, M. A. Kiskin, A. S. Bogomyakov, E. A. Suturina, A. M. Sheveleva, V. I. Ovcharenko, K. Holldack, C. Herrmann, M. V. Fedin, A. Schnegg, S. L. Veber, *J. Mater. Chem. C* **2021**, *9*, 9446.
[83] J. Pilbrow, *J. Magn. Reson.* **1978**, *31*, 479.
[84] L. Banci, A. Bencini, C. Benelli, D. Gatteschi, C. Zanchini, Spectral-structural correlations in high-spin cobalt(II) complexes, in *Structures versus Special Properties*, pages 37–86, Springer Berlin Heidelberg, Berlin, Heidelberg **1982**.
[85] H. Drulis, K. Dyrek, K. Hoffmann, S. K. Hoffmann, A. Weselucha-Birczynska, *Inorg. Chem.* **1985**, *24*, 4009.
[86] D. V. Korchagin, Y. E. Gureev, E. A. Yureva, G. V. Shilov, A. V. Akimov, E. Y. Misochko, R. B. Morgunov, K. V. Zakharov, A. N. Vasiliev, A. V. Palii, T. Lohmiller, K. Holldack, S. M. Aldoshin, *Dalton Trans.* **2021**, *50*, 13815.
[87] N. F. Chilton, R. P. Anderson, L. D. Turner, A. Soncini, K. S. Murray, *J. Comput. Chem.* **2013**, *34*, 1164.
[88] E. T. Spielberg, A. Gilb, D. Plaul, D. Geibig, D. Hornig, D. Schuch, A. Buchholz, A. Ardavan, W. Plass, *Inorg. Chem.* **2015**, *54*, 3432.
[89] C. E. Jackson, I. P. Moseley, R. Martinez, S. Sung, J. M. Zadrozny, *Chem. Soc. Rev.* **2021**, *50*, 6684.
[90] L. Gu, R. Wu, *Phys. Rev. B* **2021**, *103*, 014401.
[91] N. Aliaga-Alcalde, R. S. Edwards, S. O. Hill, W. Wernsdorfer, K. Folting, G. Christou, *J. Am. Chem. Soc.* **2004**, *126*, 12503.

Manuscript received: April 20, 2024
Accepted manuscript online: August 13, 2024
Version of record online: October 16, 2024